Electronic Supplementary Information

Transition from perovskite to misfit-layered structure materials: A highly oxygen deficient and stable oxygen electrode catalysts

Muhammad Saqib [a], In-Gyu Choi [b], Hohan Bae [c], Kwangho Park [a], Ji-Seop Shin [a], You-Dong Kim [a], John-In Lee [a], Minkyeong Jo [a], Yeong-Cehol Kim [b], Kug-Seung Lee [c], Sun-Ju Song [d, *], Eric D. Wachsman [e, *], Jun-Young Park [a,*]

[a] *HMC, Department of Nanotechnology and Advanced Materials Engineering, Sejong University, Seoul 05006, Korea*

[b] *School of Energy Materials and Chemical Engineering, Korea University of Technology and Education, Cheonan 31253, Korea*

[c] *Pohang Accelerator Laboratory, Pohang 37673, Korea*

[d] *Department of Materials Science and Engineering, Chonnam National University, Gwangju 61186, Korea*

[e] *Maryland Energy Innovation Institute, Department of Materials Science and Engineering, University of Maryland, College Park, MD 20742, United States*

* Correspondence and requests for materials should be addressed to J.-Y. Park (email: jyoung@sejong.ac.kr), E. D. Wachsman (email: ewach@umd.edu), and S.-J. Song (email: song@chonnam.ac.kr).

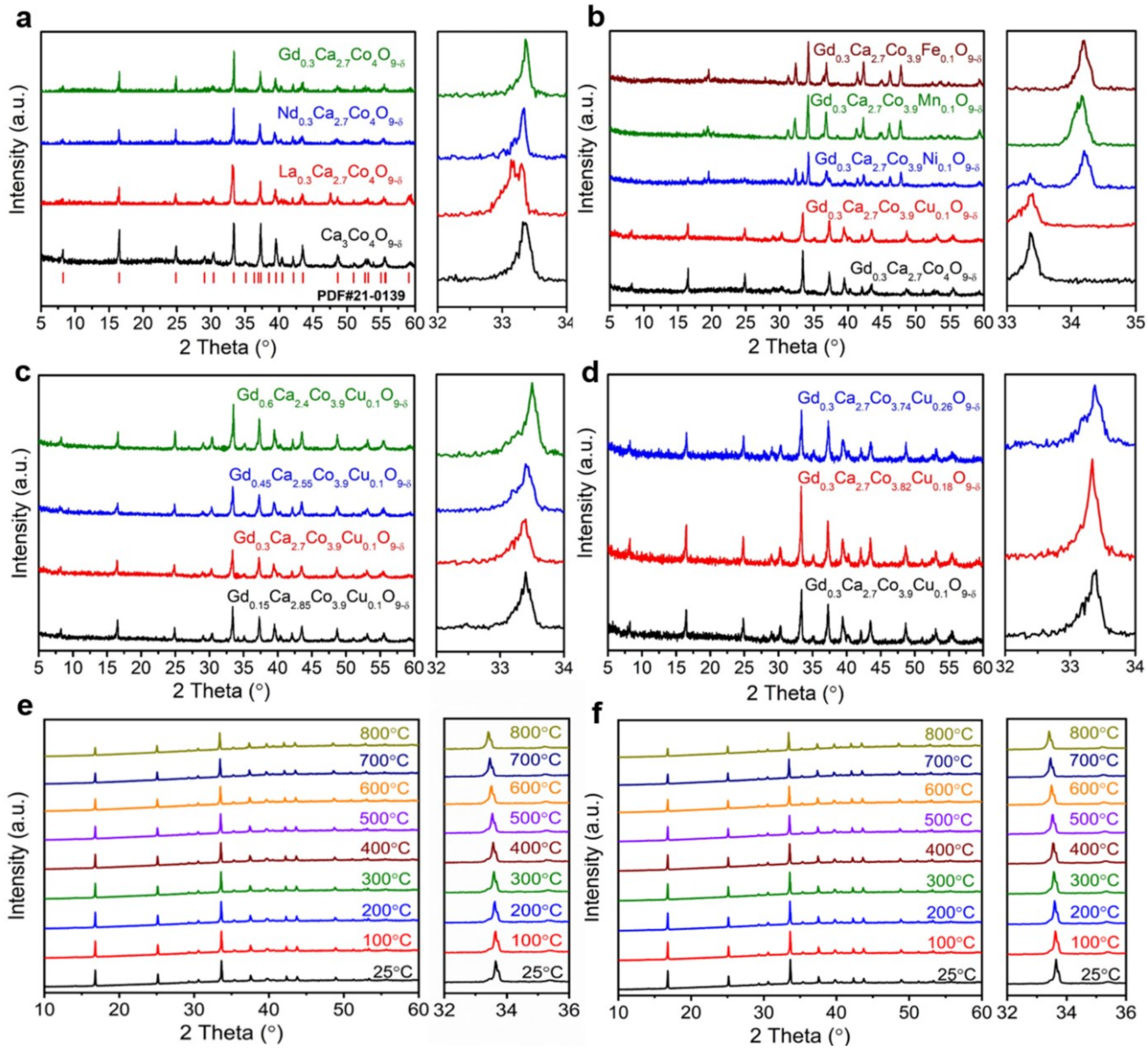

Fig. S1 Structural and phase analyses of the misfit-layered compound $Ln_xCa_{3-x}Co_{4-y}Tr_yO_{9-\delta}$ [Ln = Gd, Nd, and La (x = 0, 0.15, 0.3, 0.45, and 0.6), Tr = Fe, Mn, Ni, and Cu (y = 0, 0.1, 0.18, and 0.26)] by using XRD. (a) CCO and Ca-site doping in $Ln_{0.3}Ca_{2.7}Co_4O_{9-\delta}$ with lanthanides (Ln = Gd, Nd, and La). (b) Co-site doping in $Gd_{0.3}Ca_{2.7}Co_{3.9}Tr_{0.1}O_{9-\delta}$ with transtion metal elements (Tr = Fe, Mn, Ni, and Cu). (c) Optimization of Gd content in $Gd_xCa_{3-x}Co_{3.9}Cu_{0.1}O_{9-\delta}$ (x = 0.15, 0.3, 0.45, and 0.6). (d) Optimization of Cu content in $Gd_{0.3}Ca_{2.7}Co_{4-y}Cu_yO_{9-\delta}$ (y = 0.1, 0.18, and 0.26). (e-f) High-temperature XRD patterns of the GCCCO at temperature range from room temperature to 800℃ under dry air (e) and wet (3% H_2O) air (f).

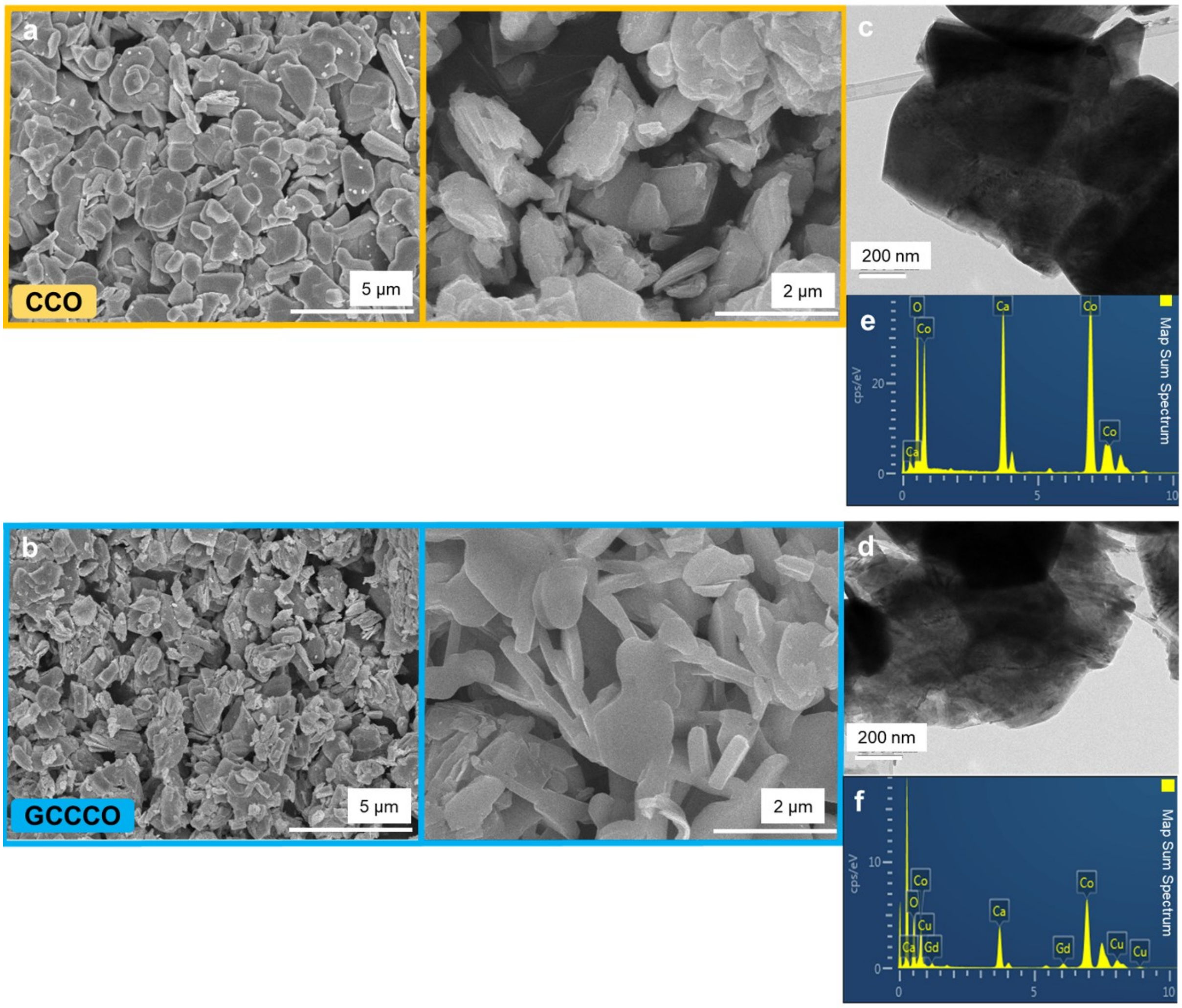

Fig. S2 Morphology characterization and elemental analyses of CCO and GCCCO. (a-b) FESEM images of CCO (a) and GCCCO (b). (c-d) HRTEM images of CCO (c) and GCCCO (d). (e-f) EDX spectra of each element in CCO (e) and GCCCO (f).

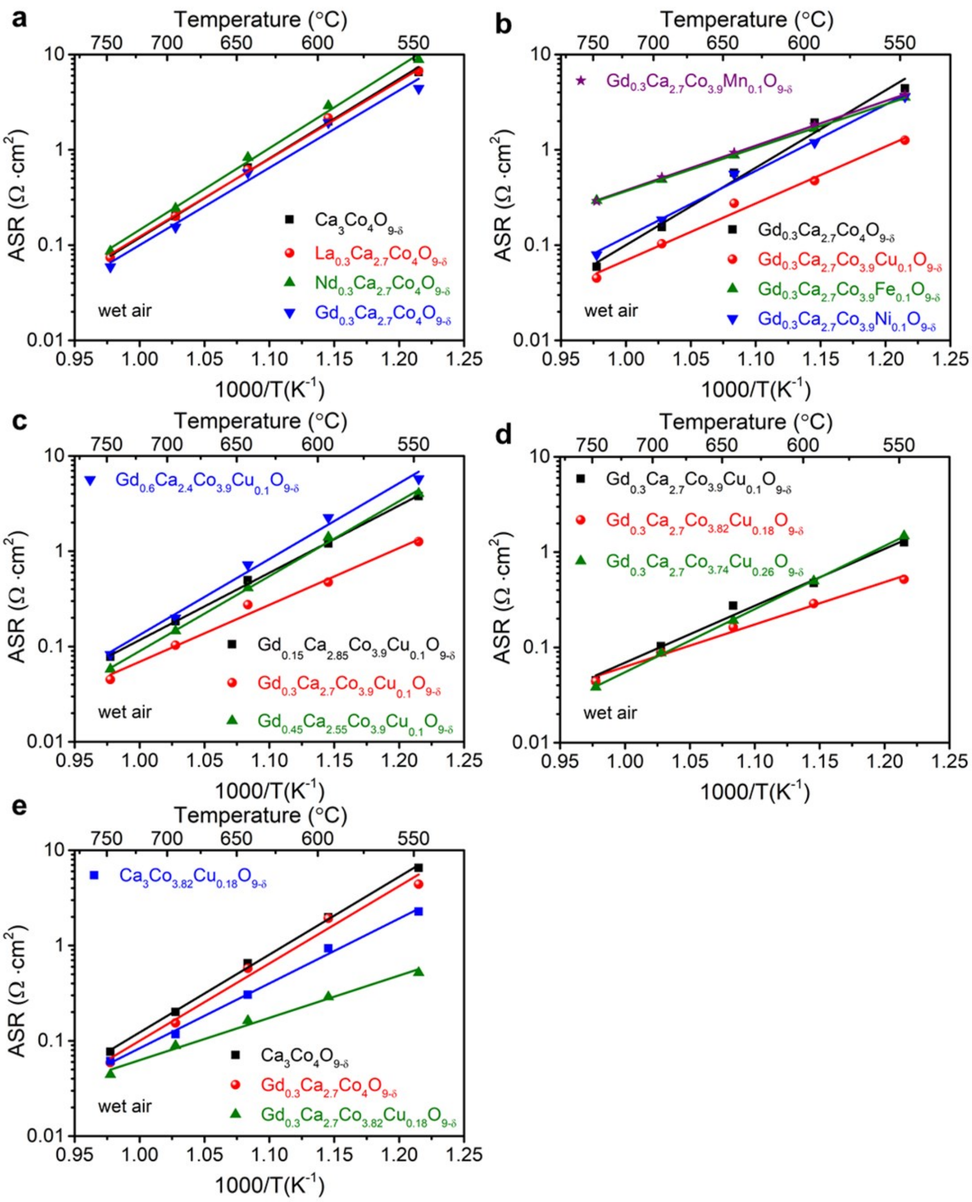

Fig. S3 Electrode ASRs in BCZYYb symmetrical cells as a function of temperature in wet air (3% H_2O). (a) Lanthanide- (Ln = La, Nd and Gd) doped $Ln_{0.3}Ca_{2.7}Co_4O_{9-\delta}$. (b) Transition metal- (Tr = Fe, Mn, Ni, and Cu) doped $Gd_{0.3}Ca_{2.7}Co_{3.9}Tr_{0.1}O_{9-\delta}$. (c) Variation of Gd doping content in $Gd_xCa_{3-x}Co_{3.9}Cu_{0.1}O_{9-\delta}$ (x = 0.15, 0.3, 0.45, and 0.6). (d) Variation of Cu doping content in $Gd_{0.3}Ca_{2.7}Co_{4-y}Cu_yO_{9-\delta}$ (y = 0.1, 0.18, and 0.26). (e) comparisons of $Ca_3Co_4O_{9-\delta}$ (CCO), $Gd_{0.3}Ca_{2.7}Co_4O_{9-\delta}$, (GCCO), $Ca_3Co_{3.82}Cu_{0.18}O_{9-\delta}$ (CCCO), and $Gd_{0.3}Ca_{2.7}Co_{3.82}Cu_{0.18}O_{9-\delta}$ (GCCCO) in electrical conductivity.

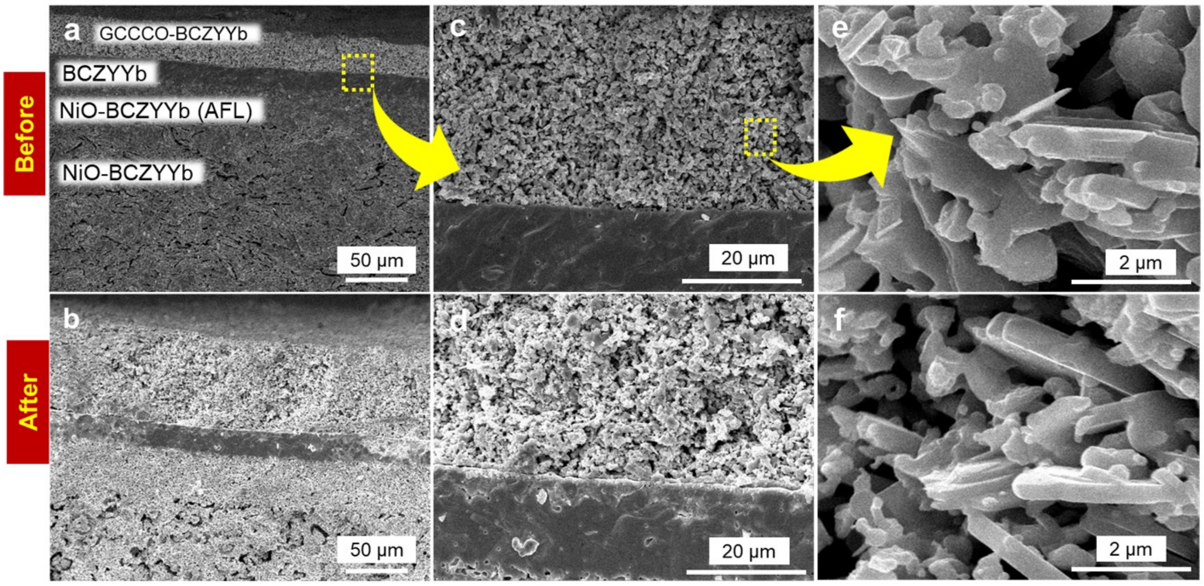

Fig. S4 Microstructural analyses of NiO-BCZYYb-supported cell with BCZYYb electrolyte and GCCCO-BCZYYb composite air/steam electrode by using FESEM. (a-b) Cross-sectional view of the as-prepared NiO-BCZYYb single cell (a) and after durability tests (b). (c-d) Interfacial region between air electrode and electrolyte before (c) and after durability tests (d). (e-f) GCCCO-BCZYYb composite air (steam) electrode before (e) and after durability tests (f).

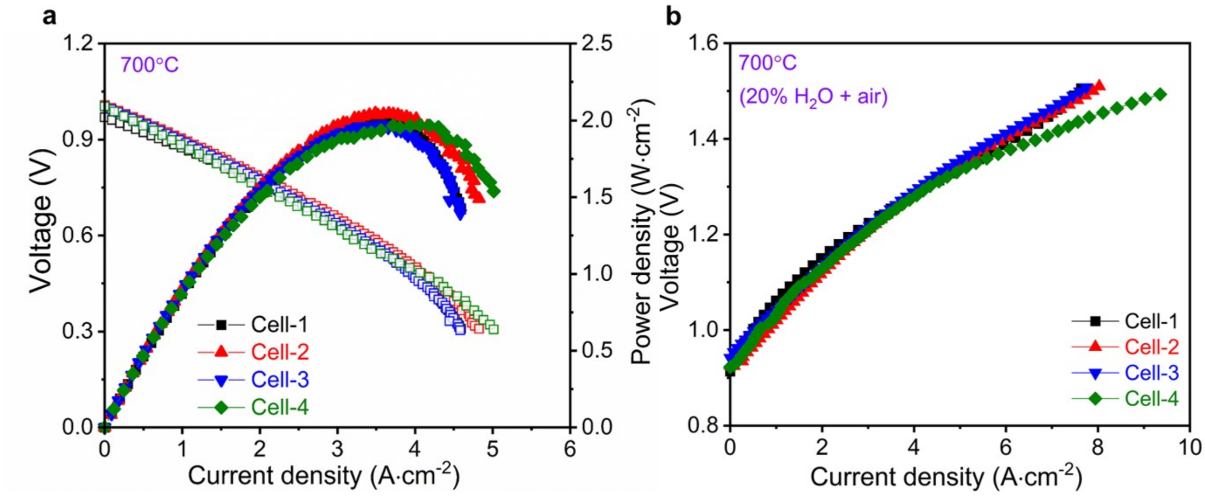

Fig. S5 Reproducibility of NiO-BCZYYb anode-supported cells with a composite GCCCO-BCZYYb air electrode. (a-b) Cell voltage as functions of current density in multiple tests at 700℃ under PCFC (a) and PCEC modes (b).

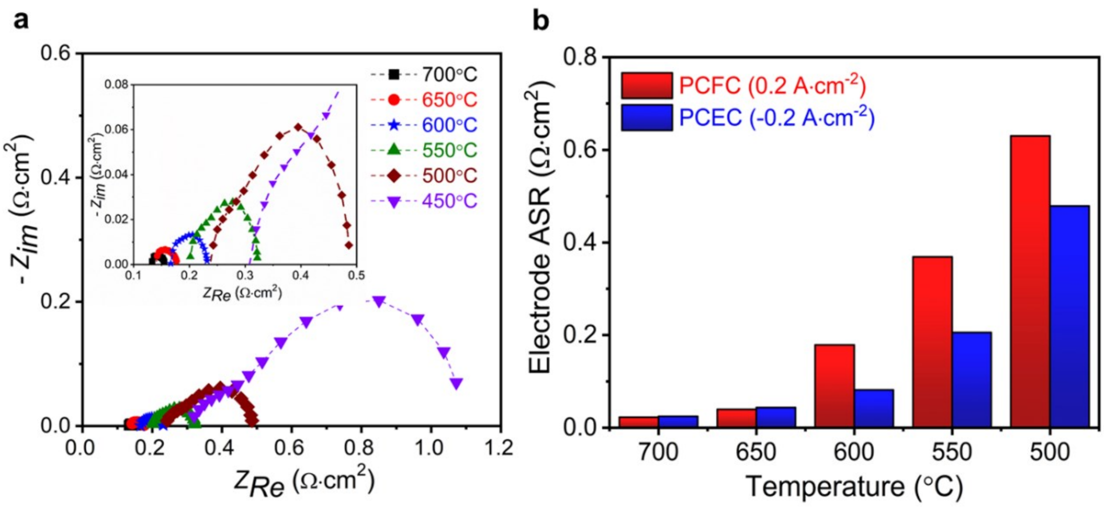

Fig. S6 EIS spectra and comparison of electrode ASR of an anode-supported GCCCO cell under PCFC and PCEC modes. (a) EIS in PCFC mode under OCV condition at 450–700℃. (b) Electrode ASRs for PCFC and PCEC mode at 0.2 A·cm^{-2} and –0.2 A·cm^{-2} conditions.

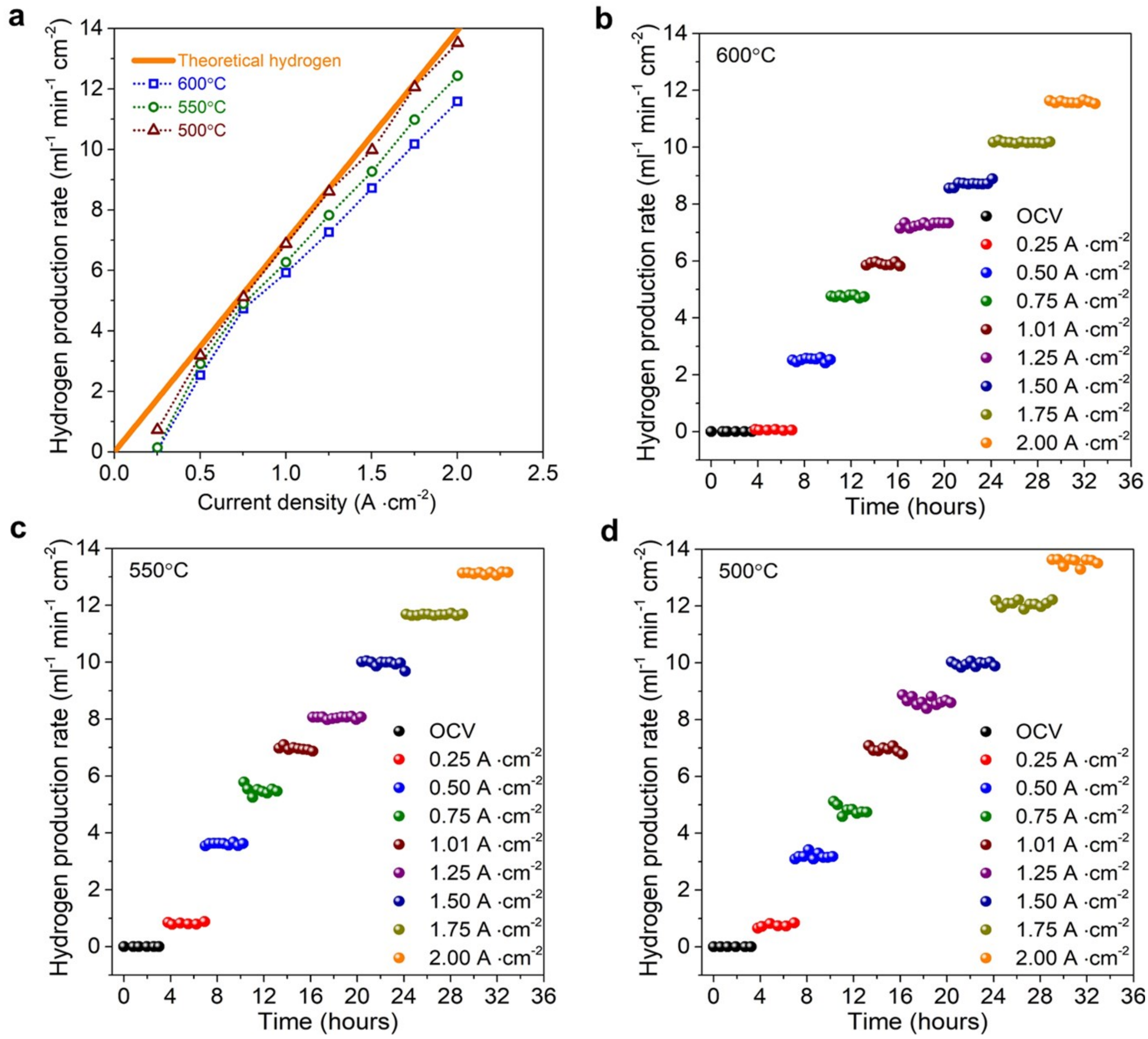

Fig. S7 Hydrogen production rate of GCCCO cell as a function of current density at 500–600℃. (a) Hydrogen production rate as a function of current density at 500–600℃. (b-d) Hydrogen production rate as a function of time under various current density at 600 (b), 550 (c), and 500℃ (d).

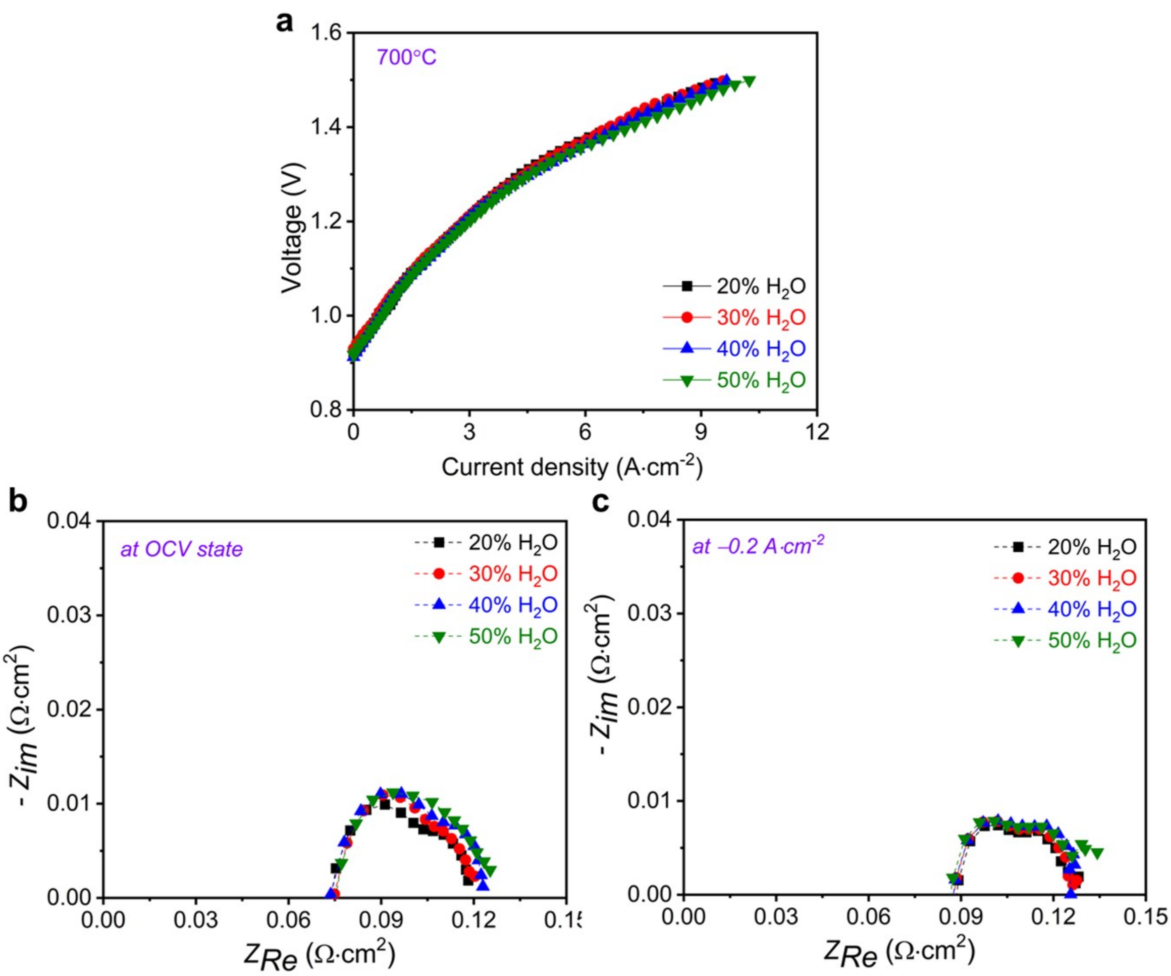

Fig. S8 Electrochemical performances of the RPCC in PCEC mode under various steam concentrations (20–50% H_2O in ambient air) at 700 °C. (a) I-V curves of a GCCCO cell. (b) EIS in PCEC mode under OCV condition. (c) EIS in PCEC mode under –0.2 A·cm^{-2} condition.

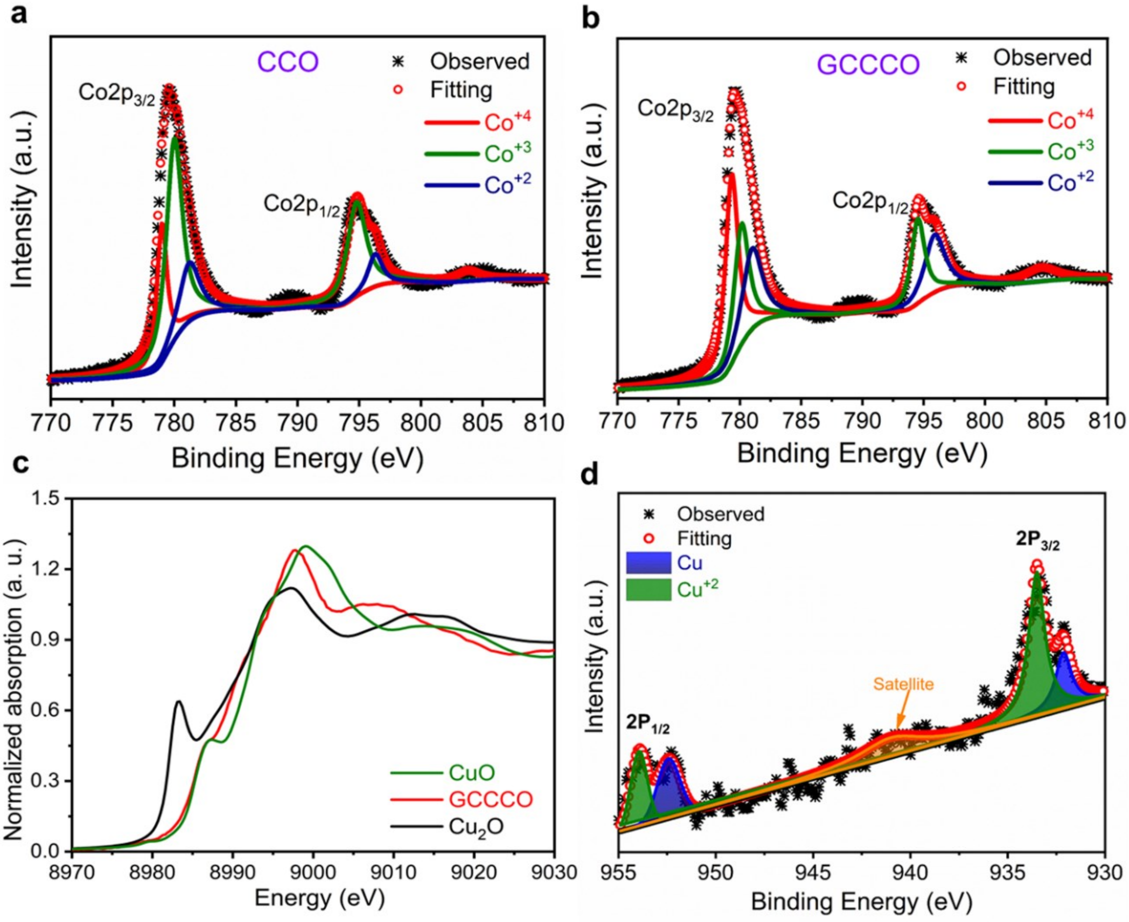

Fig. S9 XPS and X-ray absorption near edge structure (XANES) survey spectra of GCCCO materials. (a-b) Deconvoluted Co 2*p* XPS spectra for CCO (a) and GCCCO (b) materials. (c) Cu K-edge XANES spectra of GCCCO and Cu references (CuO and Cu_2O). (d) Deconvoluted Cu 2*p* XPS peaks for GCCCO.

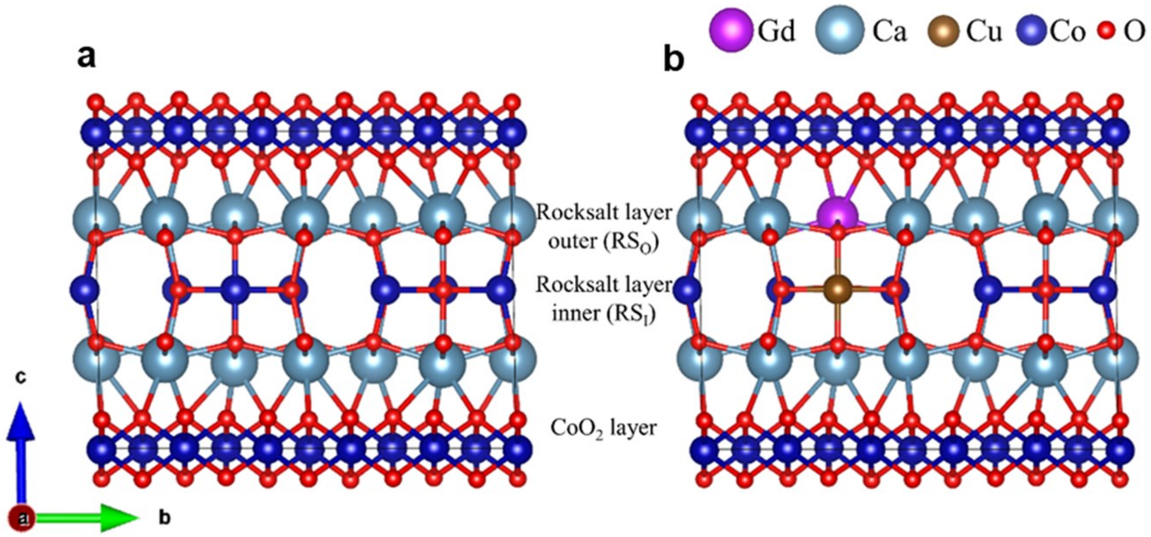

Fig. S10 The optimized misfit-layered structures. (a) CCO. (b) GCCCO. There are two nonequivalent oxygen sites at $CaCo_2O_3$ rocksalt layer (inner and outer) and one oxygen site at CoO_2 layer.

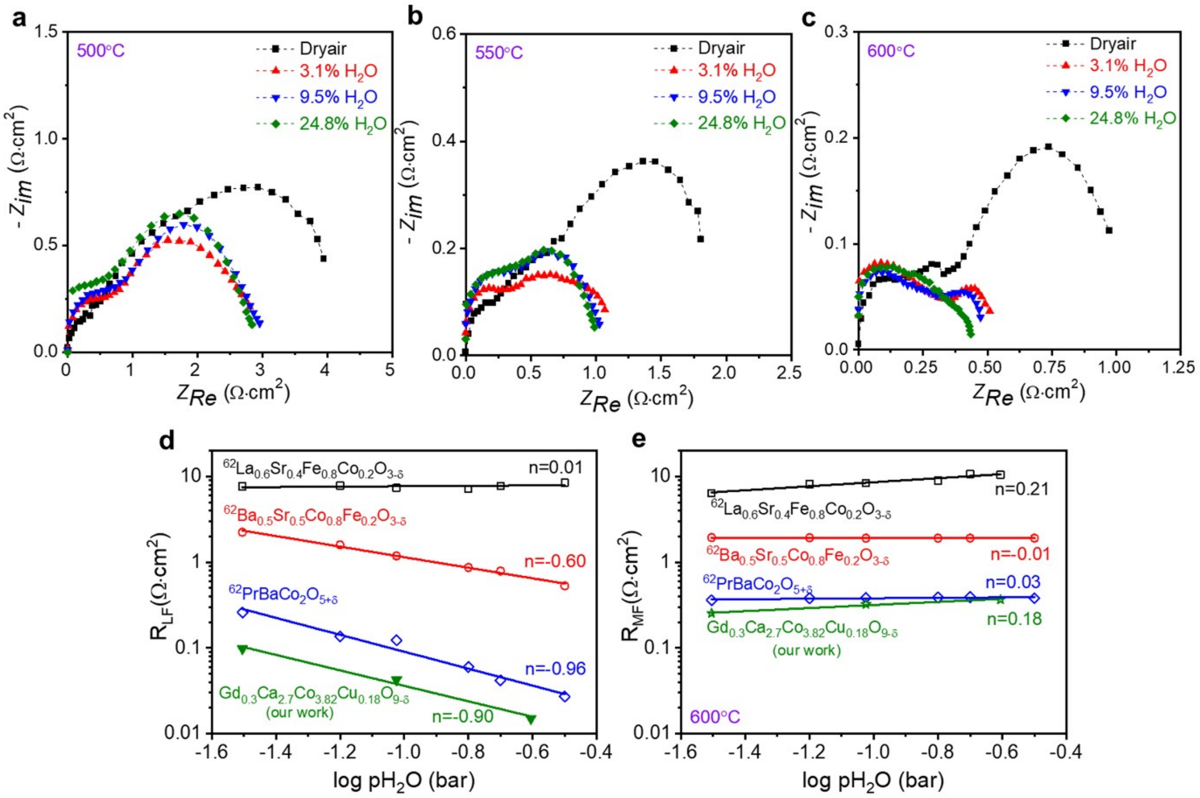

Fig. S11 EIS spectra and polarization resistance (R_p) for GCCCO under different pH_2O conditions. (a-c) EIS spectra for GCCCO at 500℃ (a), 550℃ (b), and 600℃ (c). (d-e) pH_2O dependences of R_p of various oxygen electrodes at 600℃ in low frequency (LF) (d) and middle frequency (MF) ranges (e).

Table S1 The lowest formation energy of oxygen vacancies at nonequivalent oxygen sites at $E_{Fermi} = 0$ eV.

Oxygen sites / Materials	RS_I (eV)	RS_O (eV)	CoO_2 layer (eV)
CCO	3.14	3.64	3.89
GCCCO	2.19	2.57	3.15